Start-up of oscillating heat pipes via Hopf bifurcation

Carmen Chicone, Z.C. Feng, Stephen J. Lombardo, David G. Retzloff

Start-up of oscillating heat pipes via Hopf bifurcation

Carmen Chicone

Department of Mathematics,
University of Missouri,
MO 65211, Columbia
Email: ChiconeC@missouri.edu

Z.C. Feng

Department of Mechanical and Aerospace Engineering,
University of Missouri,
MO 65211, Columbia
Email: FengF@missouri.edu

Stephen J. Lombardo*

Department of Mechanical and Aerospace Engineering,
University of Missouri,
MO 65211, Columbia
and
Department of Biomedical, Biological and Chemical Engineering,
University of Missouri,
MO 65211, Columbia
Email: LombardoS@missouri.edu
*Corresponding author

David G. Retzloff

Department of Biomedical, Biological and Chemical Engineering,
University of Missouri,
MO 65211, Columbia
Email: RetzloffD@missouri.edu

Abstract: Phase changes occur in oscillating heat pipes (OHPs) inside a tube partially filled with liquid that loops through the hot and cold zones of the device. Evaporation occurs in the hot zone, condensation in the cold zone. Their net effect would intuitively lead to accumulation of liquid slugs in the cold zone and flow stagnation. In recent work, however, self-oscillations observed in a single-branch heat pipe are explained as self-excited mechanical resonator motion. We extend their analysis to typical OHP geometry. Based on a model that combines slug dynamics with a phenomenological model of evaporation, linear stability of the equilibrium corresponding to liquid slugs filling up the cold zone of the heat exchanger is analysed. Our results

reveal relations among the system parameters that determine stability and oscillatory behaviour via Hopf bifurcations. Thus, an explanation is proposed for successful start-up – one of the grand challenges for OHP design.

Biographical notes: Carmen Chicone is an Emeritus Professor of Mathematics at the University of Missouri. He has over 45 years of teaching experience and mentored many MS and PHD students. He has published over 90 refereed journal articles and three books (most recently *An Invitation to Applied Mathematics*, Elsevier, 2017), organised conferences, and was awarded several national grants. In addition, he has served in an editorial role for several journals.

Z.C. Feng received his PhD from the University of Minnesota He is on the faculty of Department of Mechanical and Aerospace Engineering at University of Missouri. His research areas are nonlinear dynamics and chaos theory, microelectromechanical systems (MEMS), and mathematical modelling of physical systems. He is a Fellow of American Society of Mechanical Engineers.

Stephen J. Lombardo is a Professor of Mechanical Engineering with a joint appointment in Chemical and Biomedical Engineering at the University of Missouri. His PhD is from the University of California, Berkeley, followed by post-doctoral work at the Fritz Haber Institute of the Max Planck Society in Germany. He has over 25 years of teaching experience and mentoring graduate students. His research is in ceramic materials, ceramic processing, transport phenomena, and kinetics.

David G. Retzloff is an Emeritus Associate Professor in the Department of Chemical Engineering at the University of Missouri, Columbia. He earned his PhD in Chemical Engineering in the field of chemical reactions at the University of Pittsburgh and performed post-doctoral work at the University of Delft, the Netherlands. He has over 45 years of teaching experience and mentoring graduate students. He has published over 60 journal articles and conference proceedings.

1 Introduction

Oscillating heat pipes (OHPs), which were invented by Akachi (1993) and are also called pulsating heat pipes, are a special type of heat pipe consisting of a tube partially filled with liquid and configured as a heat exchanger with multiple serpentine turns through its hot and cold zones (see Figure 1). Efficient heat transfer is achieved through

the combined effects of phase changes – evaporation to vapour, condensation to liquid – and the forces they produce that cause oscillation of two-phase fluid between the hot and cold zones with no moving mechanical parts. The mechanism driving phase change is apparent, but satisfactory explanation of the mechanism responsible for flow pulsation has been elusive. Also, a clear explanation of successful start-up, which is the onset of desired, sustained oscillations not damped by flow resistance due to fluid viscosity, has not been given.

Several excellent reviews on OHPs have been published (see for example Faghri, 2014; Ma, 2015; Zhang and Faghri, 2008; Mameli et al., 2022). The recent comprehensive review by Nikolayev (2021) focuses on one space-dimension modelling of OHPs, which is the context of the research presented here. Subsection 3.2 of the Nikolayev (2021) review on film evaporation-condensation (FEC) models is most relevant. In particular, the one-branch model discussed there has been shown to have a surface in the parameter space bounding regions corresponding to stability and instability of equilibria in accordance with published simulations for multi-bend models (see Das et al., 2016; Rao et al., 2015; Zhang and Faghri, 2008; Rao et al., 2013; Nikolayev, 2011). We present a different model for multi-bend heat pipes and prove a similar result.

In a recent work by Tessier-Poirier et al. (2019b), a mechanism for self-oscillations was proposed for a single-branch pulsating heat pipe, which in their experiment is a straight pipe mounted horizontally with an open end and a closed end connected to a pressure sensor. At the closed end, a vapour bubble is created via external heating. Under experimentally controlled conditions that create an appropriate temperature gradient from the closed to the open end, a stable system equilibrium consisting of a vapour bubble bounded by a liquid slug was achieved. For sufficiently larger temperature gradients, the equilibrium state lost stability and bifurcated into an oscillatory regime as measured by the position of the liquid meniscus bounding the vapour bubble. They developed a mathematical model of their system and showed by linear stability analysis that the corresponding model has an equilibrium that loses stability with a sufficiently large increase in the temperature gradient. The subsequent motion included self sustained oscillations.

Our motivation is to generalise the results in Tessier-Poirier et al. (2019b) with the goal of providing a clear understanding of the onset of self sustained oscillations for OHP geometries found in commercial designs. Despite widespread applications in various technologies (Faghri, 2014; Ma, 2015; Zhang and Faghri, 2002; Daimura et al., 2016; Drolen et al., 2021; Nikolayev, 2021) and numerous studies both experimental and theoretical on both single and multi-turn OHPs (Mameli et al., 2019; Karthikeyan, 2014; Wang et al., 2015; Pouryoussefi and Zhang, 2016, 2017; Daimura et al., 2014; Sakulchangsatjatai et al., 2004; Mameli et al., 2021; Tessier-Poirier et al., 2019a), the lack of fundamental understanding of the basic self-oscillation mechanism as expressed, for example, in Nikolayev (2021): "Because of the lack of PHP understanding, it is not even clear which dimensionless groups are the most important, and which groups can be omitted from the analysis." has led us to address these issues for the 'start-up problem' recognised in the literature with the observation that OHPs tend "to not start-up or take a long time to start" (Daimura et al., 2016). This 'start-up problem' refers to flow stagnation during the temperature rise in the hot zone of the device, which prevents high rates of heat transfer being achieved with the desired operational regime, i.e., fluid oscillation between the hot and cold zones.

We introduced in Chicone et al. (2022) a model suitable for study of the start-up problem for realistic OHP designs and were able to completely analyse (with mathematical proof) the start-up problem for the case of two slugs that completely fill the cold zone of the OHP. Building on this foundation, we have extended our results to the case of many slugs.

Our model for start-up dynamics of OHPs is discussed in Section 2. It is a system of ordinary differential equations constructed to avoid the detailed and complex multi-physics of full OHP operation. Simplifying assumptions are specified that we believe are appropriate for viable modelling of the start-up problem. In particular, focus is concentrated on what is believed to be the dominant OHP operational mechanism of 'vapour-liquid separation', which is discussed by many other investigators (Ma et al., 2005; Zhang and Faghri, 2008; Das et al., 2016; Rao et al., 2013).

As expected, flow stagnation with all slugs residing in the cold zone corresponds to an equilibrium of our model. Linear stability analysis is used to prove the existence of a critical relation among system parameters that separates a change of stability corresponding to pairs of complex conjugate eigenvalues of the system matrix for the linearised equations at the equilibrium crossing the imaginary axis in the complex plane. A complete extension of the nonlinear analysis in Chicone et al. (2022) (for the case of two turns of the OHP tube and two corresponding liquid slugs filling the cold zone, which culminated in a proof of the existence of a non-degenerate Hopf bifurcation producing a stable limit cycle) seems to be out of reach using currently available mathematics. In fact, even for the case of two pairs of complex conjugate eigenvalues simultaneously crossing the imaginary axis (the so called Hopf-Hopf or double Hopf bifurcation), a complete description is not yet known. Thus, a full description of the nonlinear dynamics predicted by the model when the equilibrium losses stability is beyond the scope of this paper; instead, a complete analysis at the linear level is given for an arbitrary number of slugs.

In Subsection 3.1 we specify the critical value of the temperature gradient at which the stability of the equilibrium is neutral, we determine exactly the spectrum of the linearisation at this critical value (which includes multiple pairs of pure imaginary eigenvalues in the complex plane), and we prove that these pure imaginary eigenvalues simultaneously move to eigenvalues with positive real parts as the temperature gradient exceeds its critical value relative to the other system parameters. These results suggest that linear instability corresponds to OHP start-up. This result is general in the sense that it is independent of the geometric details of the OHP design.

Numerical simulations are discussed in Subsection 3.2. For all cases considered of an OHP design whose tube has n turns at one end, $n-1$ pairs of complex conjugate eigenvalues cross the imaginary axis as the temperature gradient increases through the bifurcation threshold. This suggests that the number of different quasi-frequencies of the unstable oscillations increases with the number of turns. These simulations of the nonlinear system suggest highly complex oscillatory behaviour when the equilibrium becomes unstable.

Based on the simple criterion proved for the onset of oscillations, we propose in Appendix A a (dimensionless) parameter that can be used to provide quantitative prediction for the onset of oscillations by taking into account design features such as the expected temperature gradient and the physical properties of the working fluid. Also in Appendices, we discuss some issues related to model validation.

2 A dynamic model for OHPs

Many models have been proposed for OHP operation in research articles (Zhang and Faghri, 2002; Daimura et al., 2016; Tessier-Poirier et al., 2019b; Ma et al., 2005; Zhang and Faghri, 2008; Das et al., 2016; Rao et al., 2013; Shafii et al., 2001; Thome et al., 2004; Peng et al., 2014; Pai et al., 2013); these are further discussed in books and reviews (Faghri, 2014; Ma, 2015; Zhang and Faghri, 2008; Nikolayev, 2021). Our approach is based on the work in Tessier-Poirier et al. (2019b), which treats a single liquid slug and a single vapour plug in a straight length of pipe with one closed and one open end. The domain is a tube of constant cross section. Figure 1 shows an example layout of the tube centre line with straight lengths separated by circular arcs, all of radius r. The straight sections are of length L except for those at the left and right ends to which have been added a length h to avoid intersecting the horizontal bottom return. The domain is conveniently defined for an arbitrary number of turns by noting the repeated 'arches' as shown in the figure. A single substance is the working fluid within the OHP and is present as liquid slugs and vapour plugs, for brevity henceforth referred to as slugs and plugs, separated by menisci (see Figure 2).

Figure 1   Schematic of an OHP with four turns on each side with dimensionless coordinates x and y being the physical coordinates xL and yL divided by L (see online version for colours)
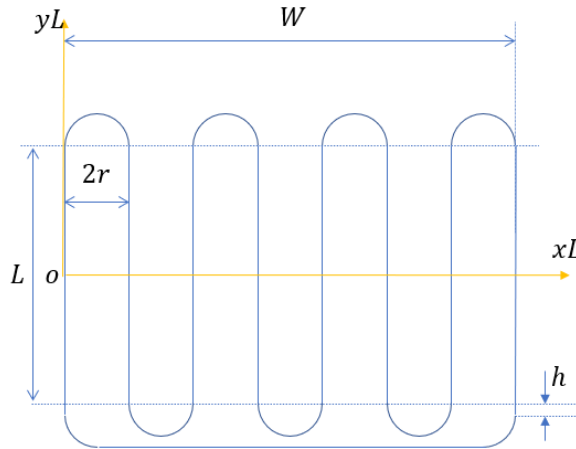
Note: To maintain the device in one plane, a vertical distance h is added to L.

We assume there are $n \geq 1$ slugs. The position of the ith slug in the OHP is represented by arc length, s_i, measured clockwise from an origin on the simple closed curve (as in Figure 1) to the meniscus on the left side of slug whose dimensionless length is denoted γ_i, where the characteristic length is L as in Figure 1 and actual lengths are depicted in Figure 2. Also, each slug is assumed to have constant density ρ; and, the same characteristic length L is used to define dimensionless plug lengths $\beta_i = l_i/L$.

The differences in pressures at the ends of each slug drive slug motion. For the ith slug, these pressures in clockwise order are given by the (uniform) plug pressures P_i and P_{i+1} assumed to be given by the ideal gas law:

$$P_i = \frac{m_i R_g T_g}{A l_i}, \tag{1}$$

where for each plug, l_i is its length, m_i is its mass, T_g is the assumed constant temperature, R_g is the specific ideal gas constant, and A is the cross sectional area of the pipe. Due to the assumed circular axial geometry of the pipe, $P_{n+1} = P_1$. Moreover, pressure is assumed to be tangentially directed along the pipe axis.

Wall drag

$$-8\pi\mu L v$$

is assumed to be due to quasi-static Poiseuille dissipation for circular cross section, characteristic length L, viscosity, μ, and velocity v.

Figure 2 Schematic diagram of liquid slugs and vapour plugs in an OHP tube with length notations (see online version for colours)
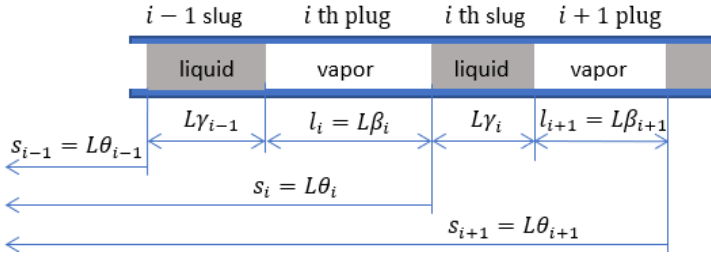
For $i = 1, 2, 3, ..., n$, the equations of slug motion become

$$\rho L \gamma_i A \ddot{s}_i = A(P_i - P_{i+1}) - 8\pi\mu L \gamma_i \dot{s}_i. \tag{2}$$

A characteristic pressure P_0 (possibly the initial vapour pressure) is used to define dimensionless quantities

$$p_i := \frac{P_i}{P_0}, \ \theta_i := \frac{s_i}{L},$$
$$\nu := \frac{8\pi L \mu}{A\sqrt{\rho P_0}}, \ \phi_i := \frac{R_g T_g}{ALP_0} m_i. \tag{3}$$

Note that the definition of ν must be adjusted if the tube cross section is not circular. Furthermore, a characteristic time

$$t_c := \sqrt{\frac{\rho L^2}{P_0}}$$

is introduced. With overdots again denoting differentiation with respect to the new dimensionless time $\tau := t/t_c$, the equations of motion in dimensionless form are

$$\gamma_i \ddot{\theta}_i = p_i - p_{i+1} - \nu\gamma_i\dot{\theta}_i, \qquad i = 1, 2, 3, ..., n, \tag{4}$$

where $p_{n+1} = p_1$.

Dimensionless pressure p is a function of dimensionless position and plug temperature. Using L_{total} to denote total pipe length and β_i the length of the ith plug,

$$\begin{aligned}
\beta_1 &= \theta_1 + \frac{L_{total}}{L} - (\theta_n + \gamma_n), \\
\beta_i &= \theta_i - (\theta_{i-1} + \gamma_{i-1}), \qquad i = 2,3,4,...,n.
\end{aligned} \tag{5}$$

We use equations (1) and (3) to represent the dimensionless pressure in the form

$$p_i = \frac{\phi_i}{\beta_i}, \tag{6}$$

where ϕ_i can be a function of temperature, T_g.

The mass of each plug m_i can change due to evaporation and condensation, and these are assumed, as in Tessier-Poirier et al. (2019b), to occur at the menisci. The rate of evaporation is further taken to be proportional to the difference between the wall temperature T_w and the local saturation temperature $T_{g,sat}$, both functions of position, evaluated at the slug menisci. The evaporation rate is therefore

$$\frac{dm_i}{dt} = \frac{T_w(\theta) - T_{g,sat}}{H_v R_{th}}, \tag{7}$$

where H_v is the latent heat of vapourisation (J/kg) and R_{th} is the thermal resistance (K/W). Equation (7) is made dimensionless with ϕ from equation (3). Retaining the same convention for dimensionless time as earlier,

$$\dot{\phi}_i = \frac{t_c R_g T_g}{A L P_0 H_v R_{th}} (T_w - T_{g,sat}). \tag{8}$$

Tessier-Poirier et al. (2019b) treats a single pipe with one open end where the pressure remains unchanged. For the OHP geometry considered here (for example as in Figure 1), the pressure at both menisci of each plug must be considered. Furthermore, evaporation and condensation need to be taken into account either by detailed modelling or by developing a phenomenological approach to replace the entire right-hand side of equation (8).

The latter approach by Chicone et al. (2022) is implemented by a judicious choice of what we call an evaporation function ev that appropriately approximates the right-hand side of equation (8) when evaluated at the positions of the menisci. More precisely, our dimensionless evaporation function is defined by

$$\mathrm{ev}(\theta) = e_v(y), \tag{9}$$

where the graph of a typical e_v (a scalar function on the real line) is depicted in Figure 3 and y is the dimensionless vertical coordinate corresponding to the second coordinate of the physical position (xL, yL) of the meniscus at θ on the OHP.

The dimensionless rate of change of vapour mass then takes the form

$$\dot{\phi}_i = \mathrm{ev}(\theta_{i-1} + \gamma_{i-1}) + \mathrm{ev}(\theta_i) \tag{10}$$

where $i = 1, 2, 3, ..., n$, $\theta_0 = \theta_n$, and $\gamma_0 = \gamma_n$. Positive rates correspond to evaporation; negative rates correspond to condensation.

Figure 3 The evaporation function versus position in the OHP (see online version for colours)
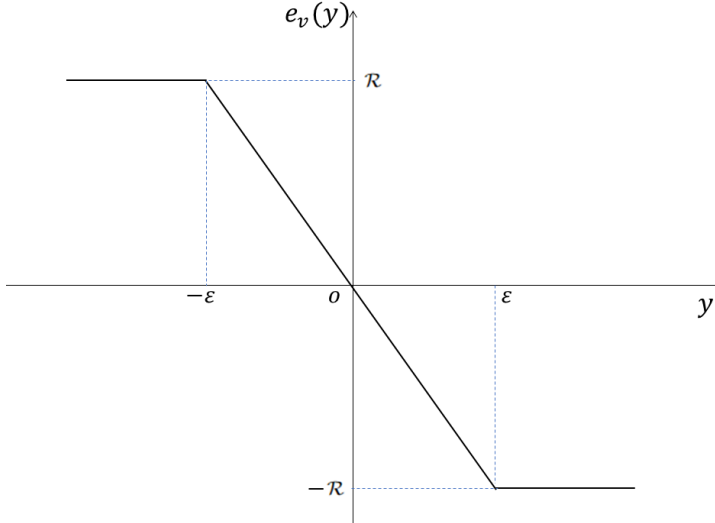
We apply equation (10) by dividing the OHP, schematically depicted in Figure 1, into three zones: a hot zone at the bottom, a cold zone at the top, and a transition region between them that is a horizontal strip of width less than $L/2$ symmetrically situated about the horizontal coordinate axis. The evaporation rate is taken to be constant and of opposite sign in the hot and cold zones, and; in the transition zone, it decreases linearly (as a function of the vertical coordinate y) making a continuous connection between the hot and cold rates. To determine e_v, the OHP wall temperature function and the (assumed constant) temperature in the vapour plugs at the menisci are taken into account. The wall temperature is assumed to be constant at T_h and T_c in the hot and cold zones, respectively. In the transition zone of width $2\epsilon L$, the constant *temperature gradient* $(T_h - T_c)/(2\epsilon L)$ is maintained. For a meniscus at equilibrium, there is no evaporation or condensation, i.e., $(T_h + T_c)/2 - T_{g,sat} = 0$. Thus we introduce

$$\mathcal{R} = \frac{t_c R_g T_g (T_h - T_c)}{2ALP_0 H_v R_{th}} \tag{11}$$

and the dimensionless parameter $\epsilon > 0$, which measures (reciprocal) steepness of the evaporation rate in the transition zone, to define the scalar function e_v on the real line by

$$e_v(y) = \begin{cases} \mathcal{R} & \text{for } y < -\epsilon, \\ -\mathcal{R}(\frac{y}{\epsilon}) & \text{for } |y| \leq \epsilon, \\ -\mathcal{R} & \text{for } y > \epsilon. \end{cases} \tag{12}$$

Here, the hot zone is in the half-plane $y < 0$ where the evaporation is positive and the cold zone corresponds to $y > 0$ where condensation occurs.

The evaporation function ev is similar in structure to the one used in Tessier-Poirier et al. (2019b) and is consistent with the near constancy of temperature in hot and cold zones and a temperature gradient in the intermediate adiabatic region as in Daimura et al. (2016).

In summary, let γ_i be the scaled length of the ith slug, ν the damping parameter, p_i the pressure at the ith meniscus, and ϕ_i the function defined in equation (3). Our dimensionless dynamical model for the motion of the position of the ith meniscus θ_i is

$$\gamma_i \ddot{\theta}_i = p_i - p_{i+1} - \nu \gamma_i \dot{\theta}_i,$$
$$\dot{\phi}_i = \text{ev}(\theta_{i-1} + \gamma_{i-1}) + \text{ev}(\theta_i) \tag{13}$$

with initial data given by scaled left-hand (with clockwise orientation in the plane) slug menisci initial positions and velocities. Here $p_i := \phi_i / \beta_i$ and ev is the evaporation function defined in equation (9).

3   Model analysis

3.1   Linearisation and onset of oscillatory motion

Near equilibrium dynamics for the case of multiple slugs and plugs in a multi-turn OHP is considered as a bifurcation phenomenon for model (13). Equilibrium occurs when all liquid slugs reside in the cold zone with all menisci at the position $y = 0$ of zero evaporation. But in the usual language of dynamical systems theory (especially when geometric objects are mentioned), equilibria are considered for a first-order system of ordinary differential equations equivalent to the model equations. Using the usual formulation by introducing velocities v_i so that $\dot{\theta}_i = v_i$, a $3n$-dimensional first-order system is obtained that is equivalent to the model equations. In equilibrium, $v_i = 0$ for $i = 1, 2, 3, ..., n$, which accounts for n independent equations. All $\dot{v}_i$ must also vanish. But this set of n equations is not independent. Due to the circular geometry, only $n - 1$ of them are independent. Likewise the vanishing of all $\dot{\phi}_i$ accounts for $n - 1$ independent equations. Thus, there is in fact a two-dimensional (invariant) manifold consisting entirely of equilibria in the $3n$-dimensional state space. Our basic result provides a criterion for the loss of stability of all these equilibria simultaneously and a linear-level description of the unstable motion: fix all system parameters except the evaporation rate $\sigma := \mathcal{R}/\epsilon$ [with $\mathcal{R}$ and ϵ as in equation (12)] and consider the stability of the equilibria with respect to changes in this parameter relative to the damping parameter ν.

Main result 3.1: As σ increases from the critical value $\sigma = \nu$, the system passes to an oscillatory regime via bifurcation due to loss of stability.

Strictly speaking, the equilibria form an attracting normally hyperbolic invariant manifold that loses stability and becomes an unstable (repelling) invariant manifold as σ increases from its critical value. This is the central result of this paper. In the unstable regime, an ignorable (measure zero) set of equilibria exists. But for a full measure set of initial data, the system evolves into unstable oscillation commensurate with start-up.

In our previous Chicone et al. (2022) paper, the case of two slugs was analysed in detail. In particular, a nondegenerate super-critical Hopf bifurcation was proved to occur; that is, a stable periodic solution exists for $\sigma > \nu$ (at least for $\sigma - \nu$ positive but sufficiently small). The proof required reduction to a centre manifold at the equilibrium of the nonlinear system in the presence of a double zero eigenvalue of the system matrix of its linearisation at the equilibrium to compute the stability index, which depends on expansion to third order of the reduced system on the centre manifold.

Application of bifurcation theory in the case of more than two slugs is much more complicated. For example, for the case of three slugs, there is a double zero eigenvalue as before but two pairs of complex conjugate eigenvalues cross the imaginary axis simultaneously as σ is increased from its critical value ν. This signals the so called Hopf-Hopf (or double Hopf) bifurcation. Numerous results in the literature prove the birth (under various circumstances) of periodic solutions, invariant tori, and chaotic dynamics, all of which meet our definition of oscillatory phenomena. As important remarks we mention two facts:

1   The full Hopf-Hopf bifurcation is co-dimension two (that is, it requires two bifurcation parameters to unfold all its phenomena)

2   Complete understanding of such bifurcations has not been achieved.

In this context, a complete picture of the bifurcation phenomena of our model is also not known even for the case of three slugs. Our main technical theorem, in support of Result 3.1, describes the structure of the spectrum of the system matrix of the linearised model equations:

Theorem 3.1: At $\sigma = \nu$, the spectrum of the $3n$-dimensional system matrix of the linearised model equations at equilibrium is decomposed as follows: $-\nu$ is an eigenvalue with multiplicity n, there is a double zero eigenvalue, and the remaining $2n - 2$ eigenvalues are all pure imaginary. Moreover, the pure imaginary eigenvalues simultaneously cross the imaginary axis, with nonzero speed, in the direction such that their real parts are positive when σ increases from ν.

This result implies that the manifold of equilibria loses stability and oscillatory motion, which we correlate with OHP start-up, occurs as σ increases from its critical value ν.

Proof: Using the obvious generalisation of the coordinates introduced in Chicone et al. (2022), the linearised system of equations at each rest point (menisci at $y = 0$ and slugs in the cold zone) takes a simple form.

To construct the linearisation of the model (13), let β_{i0} denote the dimensionless length of the ith *plug* at *equilibrium* [compare, equation (5)]. Using notation defined as in Figure 1 where the y_i are dimensionless lengths,

$$\beta_i = \beta_{i0} + y_i - y_{i-1}. \tag{14}$$

With reference to Figure 1, but for a configuration with perhaps more or fewer turns, the first plug has equilibrium dimensionless length

$$\beta_{10} = \frac{L + 2h + \pi r + 4(n-1)r}{L}. \tag{15}$$

According to our definition, the dimensionless vapour mass ϕ at equilibrium is the dimensionless plug length. Let new dimensionless variables u_i be defined by

$$\phi_i = \beta_{i0}(1 + u_i) \tag{16}$$

so that equilibrium corresponds to $u_i = 0$ and at this value $\phi_i = \beta_{i0}$ is the dimensionless equilibrium mass. Using the definition of pressure in equation (6),

$$p_i = (1 + u_i)\left[1 - \frac{y_i - y_{i-1}}{\beta_{i0}} + \left(\frac{y_i - y_{i-1}}{\beta_{i0}}\right)^2 + O\left(\left(\frac{y_i - y_{i-1}}{\beta_{i0}}\right)^3\right)\right]. \tag{17}$$

To linear order in the variables u_i and y_i, and using for notational convenience $k_i := 1/\beta_{i0}$,

$$\gamma_i \ddot{y}_i = u_i - u_{i+1} + k_i y_{i-1} - (k_i + k_{i+1}) y_i + k_{i+1} y_{i+1} - \gamma_i \nu \dot{y}_i, \tag{18}$$

where $k_{n+1} = k_1$ and $y_0 = y_n$. Also, note that each k_i is a positive real number.

The linearised evaporation equation, simplified using the two menisci bounding each vapour plug and the notation defined above, takes the form

$$\dot{u}_i = k_i(-\sigma y_i + \sigma y_{i-1}), \tag{19}$$

where as above,

$$\sigma := \frac{\mathcal{R}}{\epsilon}. \tag{20}$$

The structure of system (18)–(19) allows elimination of the auxiliary variables u_i by simply taking one further (dimensionless) time derivative to obtain a system of third-order ODEs for the positions y_i. In fact, by starting with equation (18), differentiating with respect to the temporal variable, substituting for the $\dot{u}_i$, and using the vector variable

$$Y = [y_1, y_2, y_3, ..., y_n]^T,$$

the system is (with simple algebraic manipulation) written in the matrix form

$$\dddot{Y} + \nu \ddot{Y} + W\dot{Y} + \sigma W Y = 0,$$

where $W := M^{-1}K$, $M := \text{diag}\,\gamma_i$, and

$$K := \begin{bmatrix} k_1 + k_2 & -k_2 & 0 & 0 & \cdots & 0 & -k_1 \\ -k_2 & k_2 + k_3 & -k_3 & 0 & \cdots & 0 & 0 \\ 0 & -k_3 & k_3 + k_4 & -k_4 & \cdots & 0 & 0 \\ \cdots & \cdots & \cdots & \cdots & \cdots & \cdots & \cdots \\ 0 & 0 & 0 & 0 & \cdots & k_{n-1} + k_n & -k_n \\ -k_1 & 0 & 0 & 0 & \cdots & -k_n & k_n + k_1 \end{bmatrix}. \tag{21}$$

We will show that the spectrum of the corresponding linearised $3n$-dimensional first-order system is decomposed as in the statement of the theorem.

As is usual, to compute the spectrum of the linearised system we substitute $Y = e^{\lambda t}V$ for unknown eigenvalue λ and corresponding eigenvector V to determine the vector characteristic equation

$$(\lambda^3 I + \nu\lambda^2 I + \lambda W + \sigma W)V = 0, \tag{22}$$

where I denotes the $n \times n$ identity matrix.

At bifurcation $\sigma = \nu$. For this special case, $\lambda = -\nu$ and an arbitrary n dimensional real vector V satisfies the characteristic equation. Thus, the eigenvalue $-\nu$ has (geometric) multiplicity n. Also, the existence of this root suggests that $\lambda I + \nu I$ is a factor of the equation. In fact,

$$\lambda^3 I + \nu\lambda^2 I + \lambda W + \nu W = (\lambda I + \nu I)(\lambda^2 I + W). \tag{23}$$

The two square roots (possibly complex) of each eigenvalue of W are eigenvalues of the system because of the factor $\lambda^2 I + W$. Since W is n-dimensional, this accounts for $2n$ system eigenvalues. Thus there is a total of $3n$ system eigenvalues as would be expected by writing the linearised equations as a first-order system of the form $\dot{z} = Az$ with z the $3n$-vector whose components are the y_i, $\dot{y}_i$, and u_i.

To complete the general spectral picture of the system at $\sigma = \nu$, consider the spectrum of W. By inspection each of its rows sums to zero. Thus, it has at least one zero eigenvalue. For example, the vector U, all of whose components are unity, is in the kernel. Because (in addition) all diagonal elements are positive real numbers, Gershgorin's circle theorem implies that each eigenvalue of W is zero or has positive real part. It remains to show that except for the zero eigenvalue, the remaining $n - 1$ are in fact positive real numbers.

Note that $e_1, e_2, e_3, \ldots, e_{n-1}, U$, where e_i is the usual Cartesian basis element, is a basis of the n-dimensional space. The matrix W in this basis is W with the components of its last column replaced by zeros. Thus its eigenvalues, which are the same as those of W, are zero and those of the upper left $(n - 1) \times (n - 1)$-block $\tilde{W}$. An induction argument on dimension can be constructed to prove that the determinant of $\tilde{W}$ is

$$(-1)^{n+1} \frac{2\beta_{10} + \beta_{20} + \cdots + \beta_{(n-1)0}}{\beta_{10}^2 \beta_{20} \cdots \beta_{n0} \gamma_1 \gamma_2 \cdots \gamma_n},$$

which is not zero. Thus, $\tilde{W}$ has no zero eigenvalue. The matrix $\tilde{W}$ is tridiagonal with the special property that the product of symmetric upper-diagonal and lower-diagonal elements is always positive. As is well known, such a matrix is similar to a real symmetric matrix by a similarity transformation given by a diagonal matrix. Moreover the proof is elementary. Since a symmetric matrix has real eigenvalues, the $n - 1$ nonzero eigenvalues of W are positive real numbers as promised.

Turning to the nature of the spectrum as σ increases through the critical value $-\nu$, consider first its zero eigenvalues. They do not change with σ. The matrix W, as we have seen, has a zero eigenvalue. Choose a nonzero vector U in the kernel of W and replace V by U in equation (22). The equation reduces to $\lambda^2(\lambda + \nu)U = 0$ and thus implies the existence of a double zero eigenvalue and the real eigenvalue $-\nu$ for the system independent of the value of σ. Of course, the existence of the

two-dimensional manifold of rest points to which each equilibrium belongs also implies that each linearisation has a double zero eigenvalue.

Suppose p (for positive) is an eigenvalue of W, again use the fundamental equation (22), and note that λ is a system eigenvalue exactly when it is a root of

$$\lambda^3 + \nu\lambda^2 + (\lambda + \sigma)p = 0. \tag{24}$$

At bifurcation, where $\sigma = \nu$ there is a corresponding pair of pure imaginary eigenvalues $\lambda = \pm ib$. By simply substituting into the latter equation with $\sigma = \nu$, an immediate consequence is the relation between p and b: $b^2 = p$. Next, consider the function F from the Cartesian product of the complex numbers and the real numbers to the complex numbers given by

$$F(\lambda, \sigma) = \lambda^3 + \nu\lambda^2 + (\lambda + \sigma)b^2.$$

As mentioned, $F(ib, \nu) = 0$. Also the function F is as smooth as desired; it is a polynomial. To apply the implicit function theorem, consider the partial derivative with respect to the first variable at the given zero; it is (using subscript notation for partial derivatives)

$$F_\lambda(ib, \nu) = -2b^2 + 2\nu bi,$$

a clearly nonzero value. The implicit function theorem implies that for σ in some open neighbourhood of ν, λ is a function of σ such that $\lambda(\nu) = ib$ and $F(\lambda(\sigma), \sigma) \equiv 0$ as long as λ is in this neighbourhood. By differentiating both sides of the latter equivalence with respect to σ and solving for $\lambda'(\nu)$, its value is found to be

$$\lambda'(\nu) = \frac{b^2}{2(b^2 + \nu^2)} + \frac{b\nu}{2(b^2 + \nu^2)}i.$$

Using Taylor's theorem

$$\lambda(\sigma) = ib + \left(\frac{b^2}{2(b^2 + \nu^2)} + \frac{b\nu}{2(b^2 + \nu^2)}i\right)(\sigma - \nu) + O((\sigma - \nu)^2). \tag{25}$$

Because the real part of the first-order term has positive real part, the real part of the desired eigenvalue $\lambda(\sigma)$ increases from zero as σ increases from $\sigma = \nu$, exactly as desired. All pure imaginary eigenvalues cross the imaginary axis into the positive half of the complex plane as σ crosses its critical value ν. $\square$

Remark: As σ increases from $\sigma = \nu$, the positive real part in equation (25) is a meaningful quantitative measure for the growth rate of instability. For $\sigma > \nu$, its reciprocal,

$$\tau_c = \frac{2(b^2 + \nu^2)}{b^2(\sigma - \nu)}, \tag{26}$$

provides a useful dimensionless time constant for OHP start-up. Because τ_c is derived for perturbations from an equilibrium that corresponds to the OHP 'dry out' state (i.e., all liquid slugs in the cold zone), it is the time constant corresponding to the worst case start-up scenario.

Remark: There is a redundancy in model (13) as might be expected from the existence of the double zero eigenvalue and underlying circular geometry. To prove this, simply add the equations and let

$$\mathcal{S} := \sum_{i=1}^{n} \gamma_i \theta_i.$$

Using the sum of the model equations and an easy computation,

$$\mathcal{S} = c_1 + c_2 e^{-\nu t},$$

where the integration constants c_1 and c_2 can be determined from the initial data. Solving this latter equation (for instance) for θ_n and substituting the result in the model equation eliminates this state variable. But doing so breaks the symmetric structure of the model, makes it nonautonomous and functional (due to dependence on initial data), and therefore leads to a less natural development of the theory.

3.2 *Numerical simulation*

Numerical simulations using the full nonlinear model equations of course confirm the stability criteria discussed in Subsection 3.1. They also revealed more information, some of which is discussed in this section. All simulations are based on the dimensionless parameters. The characteristic length is thus set to 1. Also, the OHP size is specified by $r = 0.1$ L and $h = 0.03$ L.

Figure 4   Growth of plug pressure oscillations versus time for $\sigma \approx 0.617$ and $\nu = 0.500$ for two slugs (see online version for colours)
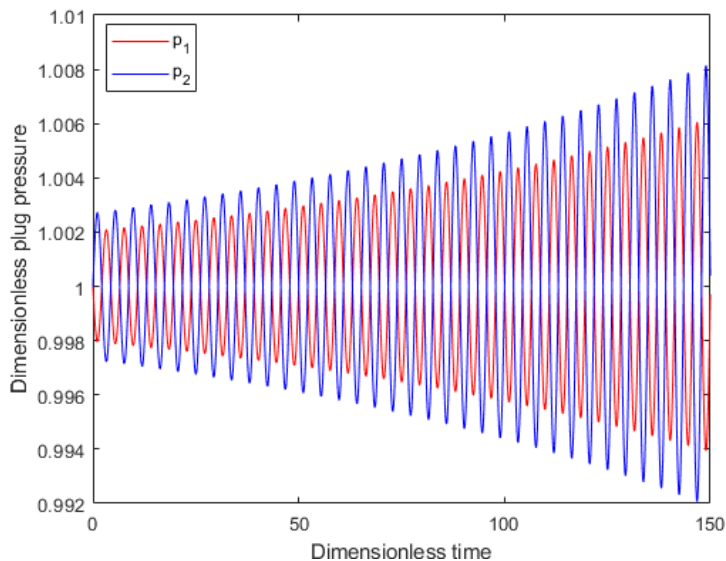
Notes: The oscillations appear to have a single frequency, which is characteristic of a standard Hopf bifurcation.

Simulation results for two, three, and five slugs completely filling the cold zone of an OHP with the corresponding number of turns on one side are reported. The two slug case with $\sigma > \nu$ shows that the near-equilibrium initial condition becomes unstable through the onset of oscillations. This can perhaps be best seen in Figure 4 where simulated plug pressure versus time is plotted for one choice of such initial data. The oscillation amplitude grows exponentially (at least over the depicted dimensionless time interval), and a single frequency characterises these oscillations.

Figure 5   Left-hand menisci positions versus time for three slugs for $\nu = 0.5$, (a) panel for $\sigma \approx 0.617$ (b) panel for $\sigma = 1.000$ (see online version for colours)

(a)   (b)
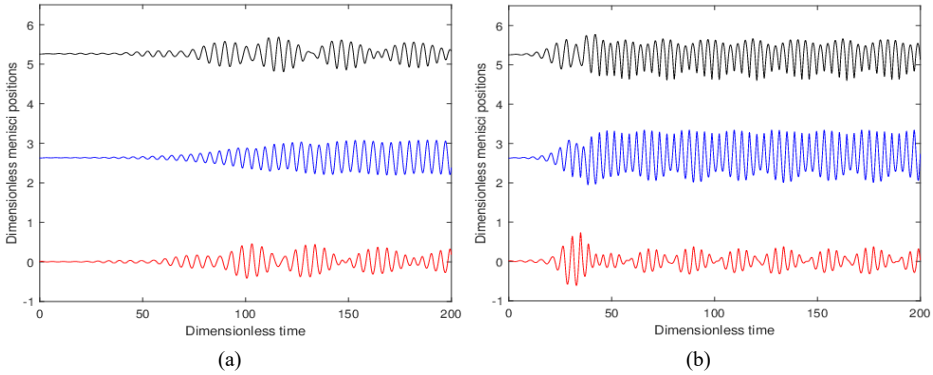
Figure 6   Left-hand menisci positions versus time for five slugs with $\nu = 0.50$, (a) panel for $\sigma = 0.65$ (b) panel for $\sigma \approx 0.834$ (see online version for colours)

(a)   (b)
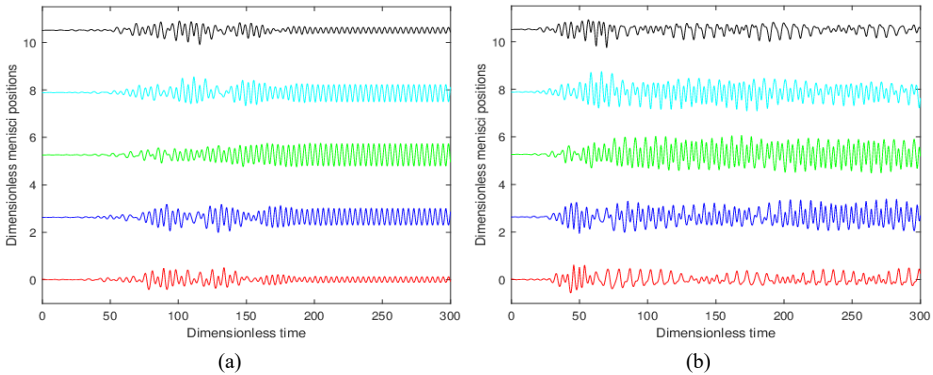
Numerically approximated graphs of the left-hand menisci positions of three slugs are depicted in Figure 5, where two frequencies are apparent, which is in concert with the theoretical results proved in Subsection 3.1. For σ near but exceeding the critical value $\sigma = \nu$, the unstable trajectory seems (due to the two-frequency quasi-periodic oscillation) to be attracted to a stable invariant torus. As the temperature gradient is increased, the oscillations increase in amplitude and the attractor seems to become more chaotic. With a sufficient increase in the temperature gradient, the oscillation amplitude increases (not shown here) until slugs merge before the observed trajectory goes to an attractor.

Numerical simulations with five slugs are depicted in Figure 6. The results are consistent with the existence of four frequencies associated with four pairs of pure imaginary eigenvalues that cross the imaginary axis as the critical value of the temperature gradient is exceeded. For small deviations of σ above its critical value, the results of our simulations suggest attraction to a stable limit cycle. But as σ increases, much more chaotic motion is observed in our simulations.

As mentioned previously, we have proved the existence of unstable oscillations in the super critical parameter regime, i.e., for $\sigma > \nu$. This is sufficient to conclude that our model predicts OHP start-up in this regime. Perhaps only of mathematical interest, an open problem is to determine more precisely the dynamics of our model for σ above but sufficiently close to ν so that slug mergers do not occur. Attraction to limit cycles, invariant tori or chaotic attractors is expected, but not proved.

References

Akachi, H. (1993) *Structure of Micro-Heat Pipe*, US Patent No. US5219020A, 15 June.

Chicone, C., Feng, Z.C., Lombardo, S.J. and Retzloff, D.G. (2022) 'Onset of oscillations driven by temperature gradients in oscillatory heat pipes', *Journal of Vibration Testing and System Dynamics*, Vol. 6, No. 3, pp.247–271.

Daimaru, T., Nagai, H., Ando, M., Tanaka, K., Okamoto, A. and Sugita, H. (2016) 'Comparison between numerical simulation and on-orbit experiment of oscillating heat pipes', *46th International Conference on Environmental Systems*, Vienna, Austria, 10–14 July, ICES-2016-185.

Daimaru, T., Yoshida, S., Nagai, H., Okamoto, A., Ando, M. and Sugita, H. (2014) 'Mathematical modeling and experimental validation of oscillating heat pumps', *44th International Conference on Environmental Systems*, Tucson, Arizona, 13–17 July.

Das, S.P., Nikolayev, V.S., Lefèvre, F., Pottier, B., Khandekar, S. and Bonjour, J. (2010) 'Thermally induced two-phase oscillating flow inside a capillary tube', *International Journal of Heat and Mass Transfer*, Vol. 53, pp.3905–3913.

Drolen, B.L. and Smoot, C.D. (2017) 'Performance limits of oscillating heat pipes: theory and validation', *Journal of Thermophysics and Heat Transfer*, Vol. 31, pp.920–936.

Drolen, B.L., Wilson, C.A., Taft, B.S., Allison, J. and Irick, K.W. (2021) 'Advanced structurally embedded thermal spreader oscillating heat pipe micro-gravity flight experiment', *Journal of Thermophysics and Heat Transfer*, Vol. 36, pp.314–327.

Faghri, A. (2014) 'Heat pipes: review, opportunities and challenges', *Frontiers in Heat Pipes*, Vol. 5, pp.1–48.

Karthikeyan, V., Khandekar, S., Pillia, B. and Sharma, P.K. (2014) 'Infrared thermography of a pulsating heat pump: flow regimes and multiple steady states', *Applied Thermal Engineering*, Vol. 62, pp.470–480.

Ma, H. (2015) *Oscillating Heat Pipes*, Springer, New York.

Ma, H.B., Hanlon, M.A., and Chen, C.L. (2005) 'An investigation of oscillating motions in a miniature pulsating heat pipe', *Microfluid Nanofluid*, Vol. 2, pp.171–179.

Mameli, M., Besagni, G. and Pradeep, P. (2021) 'Special issue: Innovations in pulsating heat pipes', *Applied Thermal Engineering*, Vol. 203.

Mameli, M., Besagni, G., Bansal, P. and Markides, C. (2022) 'Innovations in pulsating heat pipes: from origins to future perspectives', *Applied Thermal Engineering*, Vol. 203, p.117921.

Mameli, M., Catarsi, A., Mangani, L., Pietrasanta, L., Miche, N., Marengo, M., DiMarco, S. and Filippeschi, S. (2019) 'Start-up in microgravity and local thermodynamic states of a hybrid loop thermosyphon/pulsating heat pipe', *Applied Thermal Engineering*, Vol. 158, p.113771.

Nikolayev, V.S. (2011) 'A dynamic film model of the pulsating heat pipe', *Journal of Heat Transfer*, Vol. 133, p.81504.

Nikolayev, V. (2021) 'Physical principles and state-of-the-art of modeling of the pulsating heat pipe: a review', *Applied Thermal Engineering*, Vol. 195, p.117111.

Pai, P.F., Peng, H. and Ma, H. (2013) 'Thermomechanical finite-element analysis and dynamics characterization of three-plug oscillating heat pipes', *International Journal of Heat and Mass Transfer*, Vol. 64, pp.623–635.

Peng, H., Pai, P.F. and Ma, H. (2014) 'Nonlinear thermomechanical finite-element modeling, analysis and characterization of multi-turn oscillating heat pipes', *International Journal of Heat and Mass Transfer*, Vol. 69, pp.424–437.

Pouryoussefi, S.M. and Zhang, Y. (2016) 'Numerical investigations of chaotic flow in a 2D closed-loop pulsating heat pipe', *Applied Thermal Engineering*, Vol. 98, pp.617–627.

Pouryoussefi, S.M. and Zhang, Y. (2017) 'Analysis of chaotic flow in a 2D multi-turn closed-loop pulsating heat pipe', *Applied Thermal Engineering*, Vol. 126, pp.1069–1076.

Rao, M., Lefèvre, F., Khandekar, S. and Bonjour, J. (2013) 'Understanding transport mechanism of a self-sustained thermally driven oscillating two-phase system in a capillary tube', *International Journal of Heat and Mass Transfer*, Vol. 65, pp.451–459.

Rao, M., Lefèvre, F., Khandekar, S. and Bonjour, J. (2015) 'Heat and mass transfer mechanisms of a self-sustained thermally driven oscillating liquid-vapour meniscus', *International Journal of Heat and Mass Transfer*, Vol. 86, pp.519–530.

Sakulchangsatjatai, P., Terdtoon, P., Wongratanaphisan, T., Kamonpet, P. and Murakami, M. (2004) 'Operation modeling of closed-end and closed-loop oscillating heat pipes at normal operating condition', *Applied Thermal Engineering*, Vol. 24, pp.995–1008.

Schwarz, F., Danov, V., Lodermeyer, A., Hensler, A. and Becker, S. (2020) 'Thermodynamic analysis of the dryout limit of oscillating heat pipes', *Energies*, Vol. 13, p.6346.

Shafii, M.B., Faghri, A. and Zhang, Y. (2001) 'Thermal modeling of unlooped and looped pulsating heat pipes', *Journal of Heat Transfer*, Vol. 123, p.1159–1172.

Tessier-Poirier, A., Rand, R. and Frechette, L.G. (2019a) 'What limits the oscillations amplitude of the single-branch pulsating heat pipe', *International Symposium on Oscillating/Pulsating Heat Pipes (ISOPHP 2019)*, Daejeon, Korea, 25–28 September.

Tessier-Poirier, A., Monin, T, Leveille, E., Monfray, S., Formosa, F. and Frechette, L.G. (2019b) 'How evaporation and condensation lead to self-oscillations in the single-branch pulsating heat pipe', *Physical Review Fluids*, Vol. 4, p.103901.

Thome, J.R., Dupont, V. and Jacobi, A.M. (2004) 'Heat transfer model for evaporation in microchannels. Part I: presentation of the model', *International Journal of Heat and Mass Transfer*, Vol. 47, pp.3375–3385.

Wang, J., Ma, H. and Zhu, Q. (2015) 'Effects of the evaporator and condenser lengths on the performance of pulsating heat pumps', *Applied Thermal Engineering*, Vol. 91, pp.1018–1025.

Zhang, Y. and Faghri, A. (2002) 'Heat transfer in a pulsating heat pipe with open end', *International Journal of Heat and Mass Transfer*, Vol. 45, pp.755–764.

Zhang, Y. and Faghri, A. (2008) 'Advances and unsolved issues in pulsating heat pipes', *Heat Transfer Engineering*, Vol. 29, pp.20–44.

Appendix A

Critical parameter for OHP start-up and sustained operation

We have introduced and discussed a parameter σ/ν related to the onset of oscillations. Based on the evidence provided by our theoretical analysis and numerical simulations, a natural postulate is the criterion $\sigma > \nu$ (or $\sigma/\nu > 1$) for successful OHP operation. The ratio of parameters $\mathcal{R}/(\epsilon\nu) = \sigma/\nu$ is independent of the detailed geometry of an OHP in our model and therefore should hold in physical OHPs. From the definitions of these parameters,

$$\frac{\mathcal{R}}{\epsilon\nu} = \frac{\rho R_g T_g}{8\pi\mu P_0 H_v R_{th}} \frac{(T_h - T_c)}{2\epsilon L}. \tag{27}$$

A perhaps surprising feature of this result is that the onset of self-oscillations is controlled by a lumped parameter that depends on the pipe geometry only through the term $(T_h - T_c)/(2\epsilon L)$, namely the temperature gradient in the OHP. Other geometric features of the OHP design do not affect the stability criterion. In fact, the remaining parameters reflect the physical properties of the working fluid and the thermal resistance.

Appendix B

Model validation

Many experimental results are reported in the literature on OHPs; but, due to a lack of standardisation and omitted details, comparisons are difficult if not impossible to make with confidence. Nonetheless, we have attempted to validate the criterion $\sigma > \nu$ using published data.

To apply equation (27) for successful OHP design (one hot zone and one cold zone separated by a transition region) reported in Daimura et al. (2016) with R-134a working fluid, our analysis necessarily involves some estimations, most significant of which is the representation of R_{th}. Different viewpoints are encompassed via three approaches to describe R_{th}:

1   by using published thermal resistance data (reciprocal of the thermal conductance)

2   by expressing $R_{th} = 1/(A_{ext}h)$, where h is the heat transfer coefficient with the external area calculated from the tube diameter and total tube length in the hot zone

3   by expressing $R_{th} = 1/(A_{ext}h)$, where the external area is determined from the heater footprint into the OHP.

Figure 7 shows how $\mathcal{R}/(\epsilon\nu)$ varies versus R_{th} for selected values of $(T_h - T_c)/2$, along with the critical value $\sigma/\nu = 1$ for our criterion. Regions of Figure 7 above $\sigma/\nu = 1$ correspond to successful OHP start-up, those below to unsuccessful start-up. The region of successful OHP operation reported from thermal resistance data from Daimura et al. (2016) is depicted by black squares. They all lie above $\sigma/\nu = 1$ and are therefore consistent with our result. Regions of operation corresponding to the two

representations of $R_{th} = 1/(A_{ext}h)$ are shown by the enclosed red and blue areas for h ranging from 500–3,000 W/(m²K); these areas also lie above $\sigma/\nu = 1$. Also, note that the time constant of instability, τ_c from equation (26), corresponding to $\sigma/\nu > 1$, implies that lying well above the $\sigma/\nu = 1$ line is favourable for successful OHP operation in finite time.

Figure 7 $\mathcal{R}/(\epsilon\nu)$ versus the thermal resistance, R_{th}, for different values of the temperature difference, $(T_h - T_c)/2$ (see online version for colours)
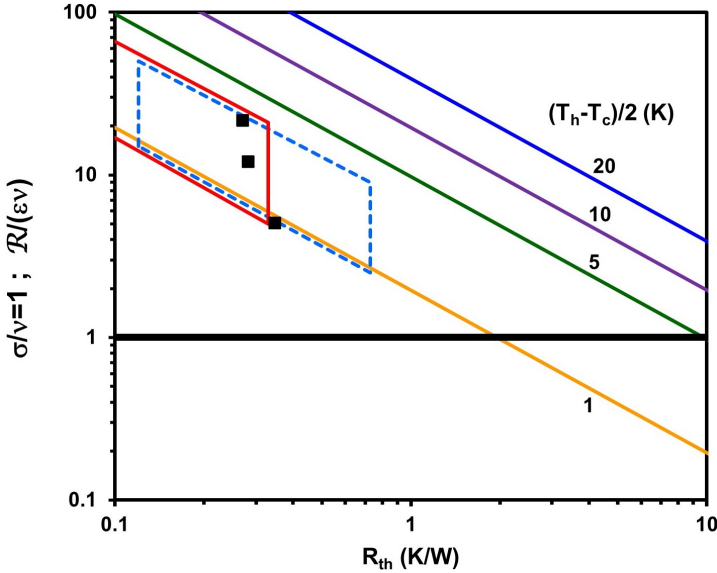
Notes: The bifurcation criterion $\sigma/\nu = 1$ is shown by the thick black line.
The estimated region of operation from Daimura et al. (2016) with working fluid R-134a is shown by the black squares (calculated from conductance data), by the dashed blue box (calculated from $R_{th} = 1/(A_{ext}h)$ using the heat input into A_{ext} = hot zone pipe periphery area) and the solid red box (calculated from $R_{th} = 1/(A_{ext}h)$ using the power input into A_{ext} = heater footprint); for the latter two methods, h was allowed to range from 500–3,000 W/(m²K).

Table 1   Comparison of one set of model parameters used in this work with three sets of data for different power inputs (and thus temperature differences) from Daimura et al. (2016)

Quantity	This work	Daimura et al. (2016)
$t_c(s)$	-	0.014
ϵ	0.3	0.0996
ν	0.5	0.107
$\mathcal{R}$	0.155	0.063, 0.122, 0.209
σ	0.51	0.63, 1.22, 2.10
σ/ν	1.03	5.85, 11.37, 10.50

As another comparison, data from the extensive ASETS-II experiments in Drolen et al. (2021) are shown in Figure 8 for 22 sets of operating conditions for both ground and in-flight tests corresponding to two OHP configurations (referred to as OHP1-large heater and OHP1-small heater, both with butane working fluid) for heat inputs ranging from 10–40 W. Once again, all of the symbols – as determined from the reported thermal conductance data – lie above the $\sigma/\nu = 1$ line.

Figure 8 $\mathcal{R}/(\epsilon\nu)$ versus the thermal resistance, R_{th}, for different values of the temperature difference, $(T_h - T_c)/2$ (see online version for colours)
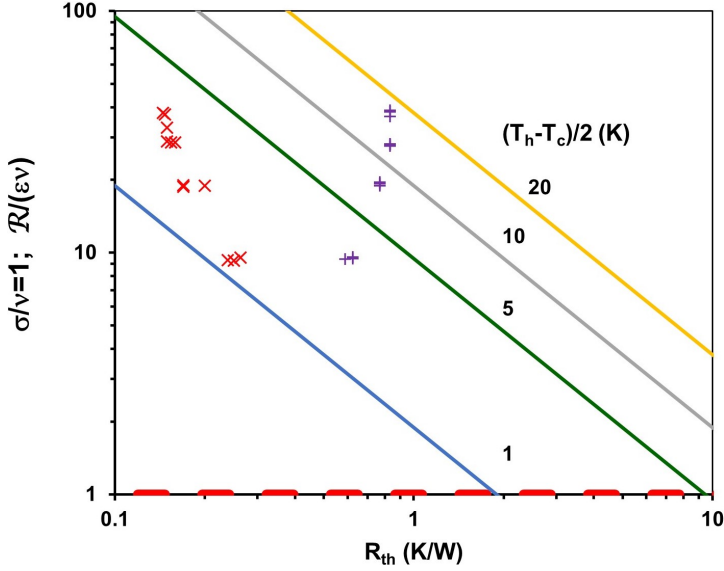
Notes: The bifurcation criterion $\sigma/\nu = 1$ is shown by the red dashed line. The estimated region of operation from Drolen et al. (2021) with butane working fluid is shown by the red x's and purple +'s for two OHP configurations.

Table 1 compares the set of parameter values used in a simulation in this work to those gleaned from the OHP data reported above in Daimura et al. (2016) for the three sets of operating conditions. The values of ϵ, ν, $\mathcal{R}$, and σ are within a factor of approximately five between the two sources. Most importantly, the desired oscillatory operational regime in this paper is $\sigma/\nu > 1$, which is again consistent with our result.

Drolen and Smoot (2017) develop design performance limits for OHPs such as the Bond limit, the vapour inertia limit, sonic limit, heat flux limit, etc. to ensure proper operation of an OHP. The results presented in this work suggest that $\mathcal{R}/(\epsilon\nu) = \sigma/\nu > 1$ is an additional performance limit that should be taken into account to obtain properly functioning OHPs.

For further comparison to published data, for the results in Figures 4–6, we estimate frequencies of 1–20 Hz using values of the characteristic time t_c computed from the data in Tessier-Poirier et al. (2019b) and Daimura et al. (2016); this frequency range lies within the observed frequencies of 0.1–20 Hz reported in Tessier-Poirier et al. (2019b), Daimura et al. (2016) and Nikolayev (2021).

An alternative view of the stability criterion is obtained by rewriting equation (27) in the form

$$\frac{\mathcal{R}}{\epsilon \nu} = \frac{\Theta}{R_f P_0 R_{th}}, \tag{28}$$

where the temperature gradient is

$$\Theta = \frac{T_h - T_c}{2\epsilon L} \tag{29}$$

and

$$R_f = \frac{8\pi \mu H_v}{\rho R_g T_g} \tag{30}$$

is a new lumped parameter containing properties of the working fluid. Minimisation of R_f is desirable to minimise the required critical start-up temperature gradient. Note that the thermal resistance R_{th} (which should be minimised) depends only on OHP physical characteristics such as tube diameter, wall thickness, and thermal conductivity (or equivalently tube diameter and heat transfer coefficient). The quantity P_0, which also should be minimised, reflects mainly the vapour pressure of the working fluid and possibly any residual inert gas pressure present in the OHP. Although not used in that sense in the model herein, P_0 may also account for superheating of the vapour. Operating at high input heat fluxes – which implies higher operating temperatures and thus vapour pressures – could also possibly dampen or eliminate oscillatory behaviour. This latter conjecture provides an alternative interpretation of the dryout phenomenon, i.e., attenuation of oscillations and poor heat transfer (Drolen and Smoot, 2017; Schwarz et al., 2020).